UAV Path Planning for Surveillance Applications: Rotary-Wing vs. Fixed-Wing UAVs

B. Jafari¹, H. Saeedi², and H. Pishro-Nik¹

¹University of Massachusetts, Amherst, MA, USA

²University of Doha for Science and Technology, Doha, Qatar Email: hamid.saeedi@udst.edu.qa, pishro@ecs.umass.edu

Abstract— In this paper, we propose various path-planning scenarios for unmanned aerial vehicles (UAV) surveillance applications, aiming to provide uniform coverage over the region of interest while minimizing mechanical energy consumption. We demonstrate that depending on the specific nature of the application, the optimal path, as well as the preferred UAV type (fixed-wing versus rotary-wing), can vary. We subsequently provide recommendations about the choice of UAV type and optimal paths for surveillance applications such as fire outbreak detection or intrusion detection. Generally, it is commonly perceived that, for a given application and path, rotary-wing UAVs consume significantly more energy than their fixed-wing counterparts. However, to our surprise, we identify scenarios where the rotary-wing UAV outperforms its fixed-wing counterpart in terms of energy consumption.

Index Terms—Path Planning, FW UAV, RW UAV, Mechanical Energy, Coverage.

I. INTRODUCTION

Unmanned aerial vehicles (UAV) have been deemed as a promising technology for many applications such as package delivery, wireless communications, as well as surveillance [1]–[3]. Based on their applications, UAVs can be deployed statically or mobile. Intuitively, utilization of moving UAVs is more challenging compared to static ones. In particular, the simpler problem of UAV positioning is elevated to a more challenging problem of finding optimal paths, herein referred to as path planning, where different utility functions such as power consumption [4], throughput [5], the traveling distance or the mission completion time [6], have to be optimized subject to different constraints.

One critical issue of UAVs is the limited onboard energy of the UAV which makes the efficient consumption of mechanical energy an important subject. For a UAV with a given battery capacity, the larger the mechanical power consumption, the shorter the flight time will be, as the UAV has to return to the base and be grounded for a while to recharge the battery.

There are two major types of UAVs, namely fixed-wing (FW) and rotary-wing (RW), which have distinctly different energy consumption models. In addition to type, the mechanical energy consumption of a UAV depends on the traveled path, speed, and acceleration of the UAV. The work of [7] provided a comprehensive closed-form formulation for the energy consumption of FW UAVs for 2-D movement as a function of the traveled trajectory, as well as instantaneous

This work was supported by National Science Foundation under grants CNS-1932326 and CNS-2150832.

speed and acceleration. This work paved the way for other 2-dimensional path planning frameworks for FW UAVs [8]. In [9], this result was used to obtain a non-user-oriented path planning framework for FW UAVs with uniform coverage and optimized energy for wireless communication applications.

On the other hand, the derivation of the consumed energy for 2-D flights of RW UAVs is much more complicated than their FW counterparts and most works were limited to special path profiles, e.g., one-dimensional paths with zero acceleration. Recently, the work of [10] provided a closed-form formulation for RW UAVs that included the effect of both velocity and acceleration on energy consumption.

As far as energy consumption is concerned, majority of the works in the literature focus on one type of UAVs for a given application and to the best of our knowledge, there is no major work that provides a comprehensive comparison between the 2 types for a given application. In fact, the common perception is that for a given application and path, RW UAVs require considerably more energy than their FW counterparts and thus, a comparison seems unnecessary, i.e., whenever possible, we had better use FW UAVs to save power, and in case we have to deploy RW, e.g., when hovering is involved in the application or for other technical reasons, we will end up paying a price for the higher energy consumption.

In this paper, our aim is to design a surveillance framework to accomplish a certain detection task such as fire outbreak, search and rescue (SAR) or a monitoring mission for intrusion detection over a given area [11]–[13] with minimum consumed energy. In all surveillance applications, it is crucial to design a path that provides a reasonably uniform coverage over the corresponding area. As such, our aim is to minimize the mechanical energy while providing a fairly uniform coverage, subject to constraints dictated by the considered surveillance scenario¹. In contrast to existing works, we consider both types of UAVs and compare their permanence in terms of energy. To our surprise, we come up with scenarios in this paper for which RW UAVs perform better in terms of energy even though no hovering on a region is on the menu. To maintain the uniform coverage, we use the spiral paths proposed in [14].

¹For example, in the fire surveillance and SAR application, there is a constraint on the detection time as any delay could have catastrophic consequences such as exponential growth of the fire or significant health damages to the victim subject to rescue. On the other hand for the intrusion detection and monitoring, the UAV speed should be limited so that high-quality pictures can be taken and processed.

As another contribution, we derive closed-from formulations of the instantaneous power when we deploy the spiral paths for both FW and RW UAVs.

This paper is organized as follows: Section II introduces the system model. Energy optimization problems are presented in Section III and in Section IV, we present the numerical results. Section V concludes the paper.

II. SYSTEM MODEL AND PRELIMINARIES

In this section, we explain the system model and review the concept of spiral paths. Then we will have a comprehensive overview of the propulsion energy consumption model for both FW and RW UAVs and we will introduce the concept of coverage probability.

A. Spiral Trajectories

The family of curves below represent a spiral family trajectory:

$$Q(s) = \left[\rho s^k cos(\zeta s), \rho s^k sin(\zeta s) \right], \qquad s \in [0, 1], \quad (1)$$

where ρ is the radius of the cell, s is an arbitrary constant i.e., $0 \le s \le 1$, and k and ζ are constants that determine the shape of the curve. Each UAV starts flying from the cell center toward the cell edge over Q(s) in τ seconds. When it reaches the cell edge, it returns to the origin on the same path and continues on curve -Q(s) to reach the other side of the edge before it returns to the origin and this action repeats continuously.

The instantaneous locations of UAVs along the flying on the spiral trajectory can be obtained by setting $s = \sqrt[2k]{\frac{t}{\tau}}$ in (1):

$$Q(t) = (x(t), y(t)) = \left[\rho\sqrt{\frac{t}{\tau}}\cos(\zeta\sqrt[2k]{\frac{t}{\tau}}), \rho\sqrt{\frac{t}{\tau}}\sin(\zeta\sqrt[2k]{\frac{t}{\tau}})\right]$$
(2)

The velocity and acceleration vectors of the UAVs are defined respectively as follows:

$$V(t) = \dot{Q}(t) = (\dot{x}(t), \dot{y}(t)),$$
 (3)

$$A(t) = \ddot{Q}(t) = (\ddot{x}(t), \ddot{y}(t)).$$
 (4)

It is proven in [14] that if the above trajectory is followed, a pretty uniform coverage is guaranteed for any arbitrary user in any location of the cell.

B. Energy Consumption Model

1) Energy Consumption Model For a FW UAV: For a FW UAV moving on a 2-dimensional plane, the energy consumption is given by [7]:

$$E =$$

$$\int_{0}^{\tau} c_{1} \|V(t)\|^{3} + \frac{c_{2}}{\|V(t)\|} \left(1 + \frac{\|A(t)\|^{2} - \frac{(A^{T}(t).V(t))^{2}}{\|V(t)\|^{2}}}{g^{2}} \right) dt + \int_{0}^{\tau} mA^{T}(t)V(t)dt,$$
(5)

where V(t) and A(t) denote the instantaneous velocity and acceleration vectors respectively, and c_1 and c_2 are two constants defined in [7].

In (5), the sum of the 2 integrands is the instantaneous power, P_{inst} , which can be written as

$$P_{inst}(t) = c_1 ||V(t)||^3 + \frac{c_2}{||V(t)||} \left(1 + \frac{||A(t)||^2 - \frac{(A^T(t).V(t))^2}{||V(t)||^2}}{g^2} \right) + mA^T(t)V(t).$$
(6)

2) Energy Consumption Model For a RW UAV: From [10], the energy consumption of a RW UAV moving on a 2-dimensional plane that flies for τ seconds can be obtained as

$$E = \int_0^\tau P_{inst}(t)dt,\tag{7}$$

where $P_{inst}(t)$ is the instantaneous total consumed power at time t. It can be obtained by calculating the vertical and horizontal power consumption, i.e.,

$$P_{inst}(t) = P_{vertical}(t) + P_{horizontal}(t).$$
 (8)

The vertical consumed power can be obtained as

$$P_{vertical} = P_0 \left(1 + \frac{3\|V(t)\|^2}{U_{tip}^2} \right) + P_i \kappa \left(\sqrt{\kappa^2 + \frac{\|V(t)\|^4}{4v_0^4}} - \frac{\|V(t)\|^2}{2v_0^2} \right)^{\frac{1}{2}},$$
(9)

where κ is defined as the thrust-to-weight ratio, i.e., $\kappa = \frac{T}{W}$ and can be expressed as

$$\kappa = \sqrt{1 + \frac{(\rho S_{FP} \|V(t)\|^2 + 2m \|A(t)\|)^2}{4W^2}}.$$
 (10)

In the above equation, P_0 and P_i are two constants defined in [15] representing the blade power and induced power in hovering status, respectively, U_{tip} is the speed of the rotor blade, v_0 is the mean rotor induced velocity in hover, $S_{FP} = d_0 s A$ is the fuselage equivalent flat plate area, W = mg is the force of gravity, with m denoting the UAV mass including all its payload, and q is the gravitational acceleration.

The horizontal consumed power can be modeled as

$$\begin{split} P_{horizontal} = & P_{\parallel}(t) + P_{\perp}(t), \\ P_{\parallel}(t) = & \left(\frac{1}{2}\rho S_{FP}V_{\parallel}^{2}(t) + mA_{\parallel}(t)\right)V_{\parallel}(t), \\ P_{\perp}(t) = & \left(\frac{1}{2}\rho S_{FP}V_{\perp}^{2}(t) + mA_{\perp}(t)\right)V_{\perp}(t), \end{split}$$

where V_{\parallel} and V_{\perp} are the speed components that are parallel and perpendicular to the UAV head direction, respectively, and they can be expressed as

$$V_{\parallel}(t) = \|V(t)\|\cos\theta_h, \quad V_{\perp}(t) = \|V(t)\|\sin\theta_h.$$
 (12)

Similarly, A_{\parallel} and A_{\perp} are the acceleration components that are parallel and perpendicular to the UAV head direction and can be written respectively as follows:

$$A_{\parallel}(t) = \|A(t)\|\cos\theta_h, \quad A_{\perp}(t) = \|A(t)\|\sin\theta_h, \quad (13)$$

where θ_h is the angle between the acceleration and velocity vector that can be expressed as

$$\theta_h(t) = \arcsin\sqrt{\left(1 - \frac{(A^T(t).V(t))^2}{\|V(t)\|^2 \|A(t)\|^2}\right)}.$$
 (14)

In addition, θ_h indicates the rotation of the UAV along the roll and pitch axis in the horizontal plane, which can be modeled as

$$\theta_h = \arctan\left(\frac{\tan R_\theta}{\tan P_\theta}\right),$$
(15)

where R_{θ} is the rotation angle along the roll axis and P_{θ} is the rotation angle along the pitch axis.

According to the above analysis, the instantaneous power consumption for RW UAVs can be finally modeled as

$$P_{inst}(t) = P_{vertical}(t) + P_{\parallel}(t) + P_{\perp}(t). \tag{16}$$

C. Coverage

The concept of coverage is initially defined for telecommunication applications where a point is considered as covered if the received power or signal-to-noise (SNR) ratio is greater than a given threshold. In the simplified path loss model, this SNR threshold directly depends on the distance between transmitter and receiver assuming an omni-directional transmitter. In other words, we assume that any point in the cell can receive the signal, but that point can be considered covered or not, depending on the SNR threshold level we set.

In this paper, for the surveillance applications, we resort to the same concept: considering UAVs which are equipped with multi-camera imaging systems or an omni-directional camera that capture images in 360° view, as suggested and implemented in many works such as [16], [17]. In this case, any point of the cell is in the camera field of view range but it is considered as covered only if it is located in a distance from the UAV which is less than a certain threshold level. Nevertheless, other scenarios can also be considered. In particular, limited field of view for the UAV built-in camera can be assumed where at any instantaneous UAV location, a limited area is viewable by the UAV even though the uncovered points are still at a resolvable distance from the UAV.

III. PATH PLANNING WITH ENERGY CONSUMPTION MINIMIZATION

In this section, we propose the general form of the optimization problem associated to different surveillance scenarios where our aim is to find a path with minimal energy while providing a fairly uniform coverage over the region. We then modify this general form depending on the considered surveillance scenario and the UAV type. We have:

$$\min_{Q(t)} E, \tag{17}$$

$$s.t. C_q: Q(t) = \left(\rho\sqrt{\frac{t}{\tau}}\cos(\zeta\sqrt[2k]{\frac{t}{\tau}}), \rho\sqrt{\frac{t}{\tau}}\sin(\zeta\sqrt[2k]{\frac{t}{\tau}})\right), \tag{18}$$

$$C_v: ||V(t)|| < V_{max}, \quad \forall \quad 0 < t \le \tau, \tag{19}$$

$$C_t: \tau < \tau_{max}, \quad \forall \quad \tau > 0.$$
 (20)

In this problem, C_q limits the path to a spiral path with parameters ζ , k, with cell radius ρ and travel time τ to provide a fairly uniform coverage on the cell. Moreover, C_v sets a limit on the maximum travel speed and C_t states that the total mission or travel time should not exceed τ_{max} . By applying C_q into (17), we end up with the following optimization problem:

$$\min_{\tau,k,\zeta} E(\tau,k,\zeta) = \min_{\tau,k,\zeta} \int_0^{\tau} P_{inst}(\tau,t,k,\zeta) dt, \qquad (21)$$
s.t. C_{v} , C_{t} .

- Closed-form formulation for $P_{inst}(\tau, t, k, \zeta)$: For the case of FW UAV, by replacing $V(t) = \dot{Q}(t)$, $A(t) = \ddot{Q}(t)$ in (6), we obtain

$$P_{inst}(\tau, t, k, \zeta) = \frac{1}{8}c_1 \left[\frac{\rho^2 (k^2 + \zeta^2(\frac{t}{\tau})^{\frac{1}{k}})}{k^2 t \tau} \right]^{\frac{5}{2}} + 2c_2 \left[1 + \frac{\rho^2 \zeta^2(\frac{t}{\tau})^{\frac{1}{k}}(k + k^2 + \zeta^2(\frac{t}{\tau})^{\frac{1}{k}})^2}{16k^4 t^3 g^2 \tau (k^2 + \zeta^2(\frac{t}{\tau})^{\frac{1}{k}})} \right] \times \frac{1}{\sqrt{\frac{\rho^2 (k^2 + \zeta^2(\frac{t}{\tau})^{\frac{1}{k}})}{k^2 t \tau}}} + \frac{m\rho^2 \left(-k^3 - (-1 + k)\zeta^2(\frac{t}{\tau})^{\frac{1}{k}} \right)}{8k^3 t^2 \tau}.$$
(22)

For the case of RW UAV, using $V(t)=\dot{Q}(t)$ and $A(t)=\ddot{Q}(t)$ we first obtain $\|V(t)\|$ and $\|A(t)\|$ respectively as follows:

$$||V(t)|| = \sqrt{\frac{\rho^2(k^2 + \zeta^2(\frac{t}{\tau})^{\frac{1}{k}})}{4k^2\tau t}},$$
 (23)

$$||A(t)|| = \sqrt{\left[\frac{\rho^2(\zeta^4(\frac{t}{\tau})^{\frac{2}{k}} + k^4 + \zeta^2(\frac{t}{\tau})^{\frac{1}{k}} + 2k^2\zeta^2(\frac{t}{\tau})^{\frac{1}{k}})}{16k^4t^3\tau}}\right]. \tag{24}$$

By replacing (23) in (9) we obtain

$$P_{vertical} = P_0 \left(1 + \frac{3\rho^2 (k^2 + \zeta^2 (\frac{t}{\tau})^{\frac{1}{k}})}{4k^2 \tau t U_{tip}^2} \right)$$
 (25)

$$+ P_i \kappa \left(\sqrt{\kappa^2 + \frac{\rho^4 (k^2 + \zeta^2 (\frac{t}{\tau})^{\frac{1}{k}})^2}{64k^4 \tau^2 t^2 v_0^4}} - \frac{\rho^2 (k^2 + \zeta^2 (\frac{t}{\tau})^{\frac{1}{k}})}{8k^2 \tau t v_0^2} \right)^{\frac{1}{2}}$$

Similarly, by replacing (23) and (24) in (11), the closed-from formulation for $P_{horizontal}$ will be obtained. As such, by replacing $P_{vertical}$ and $P_{horizontal}$ in (16), we will have the corresponding closed-from formulation for the instantaneous power of the RW UAVs. Now by replacing the instantaneous power of FW UAVs (22) and the instantaneous power of RW UAVs (16) into (21), we obtain the corresponding closed-form formulation for each case. The resulting obtained equations were too complex and lengthy to be reported here. We can take advantage of the obtained closed-form formulations to obtain optimal values for ζ , k, and τ , and consequently, optimal paths, through setting the partial derivatives to 0 and getting the extremum points, or through numerical exhaustive search.

It is important to remind that once the optimal value for E is obtained, the average power \overline{P} can be calculated as E/τ .

TABLE I: Parameters of RW UAV

UAV	P_0 (Watts)	$P_{i^{(\mathrm{Watts})}}$	U_{tip} $_{(m/s)}$	<i>v</i> ₀ (m/s)	$S_{FP(m^2)}$	$W_{(N)}$
UAV	580.65	790.67	200	7.2	0.0118	100

TABLE II: Optimized values for MEFW and MERW.

	m (Kg)	UAV Type	$\overline{P}_{ ext{(Watts)}}$	P _{peak} (Watts)	V_{max} (m/s)	ζ	k	au (s)
	10	Fixed-Wing	98.11	108.41	34.21	15.52	0.79	1151
ſ	10	Rotary-Wing	708.94	801.16	16.20	18.25	0.90	2505

We will report this instead of E in the simulation results which makes more sense from practical point of view.

In this part, we consider 6 different scenarios and their associated optimization problems. First, we assume that no constraint on mission time or maximum speed is enforced, i.e., in (21), we neglect C_v and C_t . We treat this as the baseline scenario. We name the associated problems to FW and RW cases as MEFW and MERW, respectively where ME stands for minimum energy and the last 2 letters indicate the UAV type.

The paths that are optimized in MEFW and MERW problems provide the minimum energy consumption, however, any path of Q(t) dictates a certain speed profile $V(t) = \dot{Q}(t)$ to the system and we have no control over it. In certain applications such as monitoring, the camera may need some more time over a region to detect the object of interest. As such, we have to impose the constraint C_v on the speed magnitude. We name the associated problems to FW and RW cases as $MEFW_{vc}$ and $MERW_{vc}$, respectively where vc stands for velocity-constrained.

Now we consider another situation where we have no constraint on speed but there is a limitation on the mission completion time τ . This happens in applications such as fire detection where it is crucial to cover the whole cell uniformly such that the total travel time does not exceed a certain value. Accordingly, we impose the constraint C_t and name the associated problems to FW and RW cases as $MEFW_{tc}$ and $MERW_{tc}$, respectively where tc stands for time-constrained.

IV. SIMULATION RESULTS

For simulations, we consider a FW UAV with weight m=10 kg and parameters $c_1=9.26\times 10^{-4},\ c_2=2250.$ In addition, we consider a RW UAV with weight m=10 kg and parameters $P_0,\ P_i,\ U_{tip},\ v_0$ and S_{FP} whose values are listed in Table I [15]. We consider a cell of radius $\rho=4000$ m.

We first consider the case of unconstrained trajectory optimization for both FW UAV and RW UAV. In Table II, we have reported the optimized values for ζ , k, and τ for both FW UAV and RW UAV. For both UAVs, we obtain the path with minimum energy consumption and report the consumed energy (in the form of average power) as well as the peak power over the optimized path. As can be seen, the average power consumption of the RW UAV is 7 times larger than that of its FW counterpart. This means 7 times larger flying time for FW UAVs before a recharge is necessary. This is indeed a very expected result.

In Table III, we have reported the optimized values for ζ , k, and τ for $MEFW_{vc}$ and $MERW_{vc}$ problems where

TABLE III: Optimized values for $MEFW_{vc}$ and $MERW_{vc}$

<i>m</i> (Kg)	UAV Type	$\overline{P}_{ ext{(Watts)}}$	P_{peak} (Watts)	V_{max} (m/s)	ζ	k	T (s)
10	Fixed-W.	1466.01	2211.21	5	78.54	68.09	3000
10	Rotary-W.	924.55	974.27	5	64.83	54.19	3000

TABLE IV: Optimized values for $MEFW_{tc}$ and $MERW_{tc}$

(Kg)	UAV Type	$\overline{P}_{ ext{(Watts)}}$	P _{peak} (Watts)	V_{max} (m/s)	ζ	k	au (s)
10	Fixed-Wing	101.21	112.17	38.81	7.54	0.65	600
10	Rotary-Wing	718.53	1894.71	33.75	3.46	0.70	600

we impose maximum speed of $V_{max}=5\,m/s$ (compare this with the maximum speeds of 34 and 16 m/s in Table II). We also report the consumed energy as well as the peak power corresponding to the optimized path. Note that we put a cap of 3000 seconds on travel time to get realistic results. As can be seen in \overline{P} column, in contrast to the unconstrained case where the FW UAV needs considerably less energy than RW UAV, the minimum energy consumption of the FW UAV is now 1.5 times more than that of its RW counterpart. Also, the peak power of the FW UAV is more than twice the peak power of the RW UAV. That is, RW UAVs perform better than FW UAVs in terms of energy and peak power at lower speed profiles.

In Table IV, we have reported the optimized values for the time-constrained case for FW UAV and RW UAV, i.e., $MEFW_{tc}$ and $MERW_{tc}$ problems. We set $\tau_{max}=600\,s$. Compare this value with the values that are obtained for previous scenarios which are at least twice the value of 600 seconds we set here. As can be seen, by setting $\tau_{max}=600$, the optimal value for travel time will be the same as its designated upper bound. The results are not much different from the unconstrained case and FW UAV preserves its superiority in terms of energy in this case. However, the maximum speed and peak power for the RW UAV grows drastically.

Now we investigate the coverage of the proposed schemes where we obtain the fraction of the cell coverage throughout the travel time. We set different threshold values based on the camera specs, i.e., the threshold of α means that the camera can only resolve the images which are at the distance of α meters or less. If for a given point of the cell, the distance remains more than α throughout the whole trip, that point is declared uncovered. To obtain the results, we fix the flying

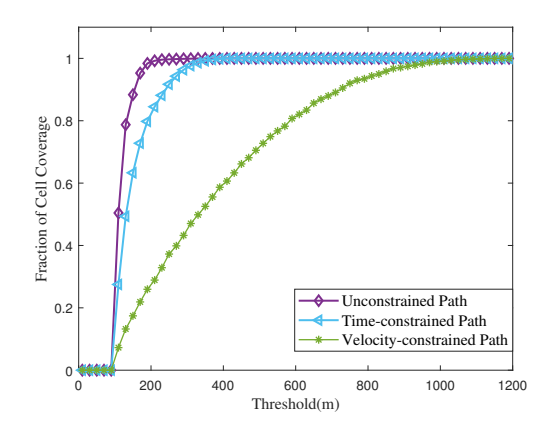


Fig. 1: Fraction of cell coverage area: FW UAV.

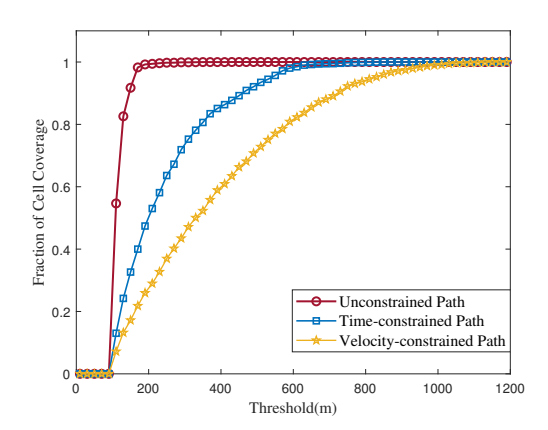


Fig. 2: Fraction of cell coverage area: RW UAV.

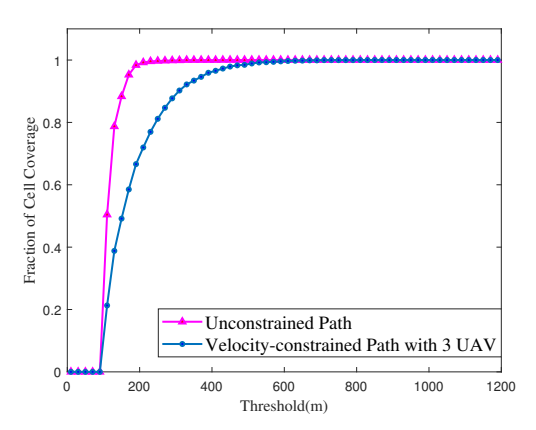


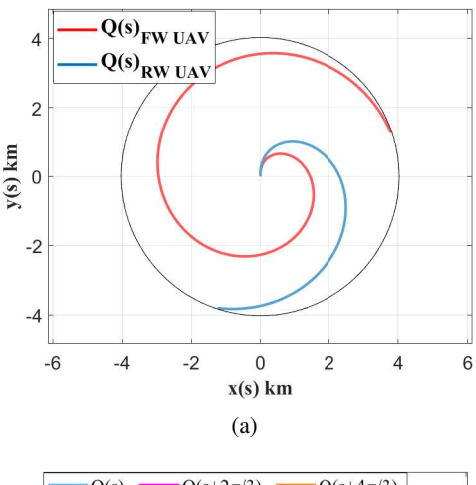
Fig. 3: Fraction of cell coverage area: unconstrained path with 1 UAV vs. velocity-constrained path with 3 UAVs.

height to 100 meters.

The results are reported in Fig. 1 and Fig. 2 for FW UAV and RW UAV, respectively. Since the flying height is set to 100 meters, for thresholds lower than this value, there will be no coverage. For the unconstrained case and for both UAV types, for thresholds greater than 100 m, full or almost full cell coverage is obtained. This will be treated as a baseline framework against which we can compare the constrained scenarios. For the time-constrained case, the threshold should be more than 200 m for the FW UAV and more than 500 m for RW UAV to get a full cell coverage.

For the velocity-constrained case, the coverage results are not acceptable if we only rely on 1 UAV, as we need cameras that should be able to resolve image of objects as far as 1 kilometer. However, we can get acceptable results if we increase the number of UAVs. As an example, for the case of velocity-constrained RW UAV, we increase the number of UAVs to 3. We have reported the results in Fig. 3. As can be seen, we have become much closer to the baseline coverage profile. We can get better results if we increase the number of UAVs even more.

In Figures 4a and 4b, we have demonstrated examples of the paths optimized in this paper. Fig. 4a corresponds to the optimized paths for the time-constrained scenario for both UAV types. In Fig. 4b, we have plotted the paths for the very last scenario where 3 RW UAVs are deployed in the velocity-constrained scenario, instead of 1, to improve the coverage.



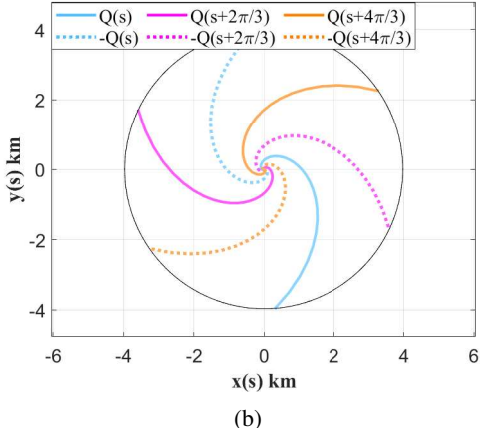


Fig. 4: (a) The optimal time-constrained path. (b) The optimal velocity-constrained path with 3 UAVs.

V. CONCLUSION

In this paper, we proposed different path planning scenarios for UAV surveillance applications, that can provide fairly uniform coverage over the region of interest, with the aim of minimizing the consumed mechanical energy. We obtained closed-form formulations for the instantaneous power over the spiral paths. Through simulations, we compared the energy consumption of both FW UAVs and RW UAVs to come up with the suitable UAV type for surveillance applications, i.e., fire breakout detection and intrusion detection. We showed that while in general, FW UAVs are preferred as far as energy consumption is concerned, there are scenarios where we have to deploy RW UAVs. This comes from the fact that RW UAVs have the ability to hover over one region in contrast to FW UAVs. This was indeed a known fact, but in this paper we showed that even if there is no hovering is on the menu, there are velocity-constrained scenarios for which RW UAVs can take over.

REFERENCES

- [1] Y. Qin, M. A. Kishk, and M.-S. Alouini, "Stochastic-geometry-based analysis of multipurpose UAVs for package and data delivery," *IEEE Internet of Things Journal*, vol. 10, no. 5, pp. 4664–4676, 2022.
- [2] X. Liu, J. Wang, N. Zhao, Y. Chen, S. Zhang, Z. Ding, and F. R. Yu, "Placement and power allocation for NOMA-UAV networks," *IEEE Wireless Communications Letters*, vol. 8, no. 3, pp. 965–968, 2019.

- [3] H. Shakhatreh, A. H. Sawalmeh, A. Al-Fuqaha, Z. Dou, E. Almaita, I. Khalil, N. S. Othman, A. Khreishah, and M. Guizani, "Unmanned aerial vehicles (UAVs): A survey on civil applications and key research challenges," *IEEE Access*, vol. 7, pp. 48 572–48 634, 2019.
- [4] H. Wang, G. Ren, J. Chen, G. Ding, and Y. Yang, "Unmanned aerial vehicle-aided communications: Joint transmit power and trajectory optimization," *IEEE Wireless Communications Letters*, vol. 7, no. 4, pp. 522–525, 2018.
- [5] Y. Zeng, R. Zhang, and T. J. Lim, "Throughput maximization for UAVenabled mobile relaying systems," *IEEE Transactions on communica*tions, vol. 64, no. 12, pp. 4983–4996, 2016.
- [6] Y. Zeng, X. Xu, and R. Zhang, "Trajectory design for completion time minimization in UAV-enabled multicasting," *IEEE Transactions on Wireless Communications*, vol. 17, no. 4, pp. 2233–2246, 2018.
- [7] Y. Zeng and R. Zhang, "Energy-efficient UAV communication with trajectory optimization," *IEEE Transactions on Wireless Communications*, vol. 16, no. 6, pp. 3747–3760, June 2017.
- [8] X. Jing, J. Sun, and C. Masouros, "Energy aware trajectory optimization for aerial base stations," *IEEE Transactions on Communications*, vol. 69, no. 5, pp. 3352–3366, May 2021.
- [9] B. Jafari, H. Saeedi, S. Enayati, and H. Pishro-Nik, "Energy-optimized path planning for moving aerial base stations: A non user-oriented framework," *IEEE Communications Letters*, vol. 26, no. 3, pp. 672–676, 2021
- [10] H. Yan, Y. Chen, and S.-H. Yang, "New energy consumption model for rotary-wing UAV propulsion," *IEEE Wireless Communications Letters*, vol. 10, no. 9, pp. 2009–2012, 2021.
- [11] A. Shamsoshoara, F. Afghah, A. Razi, S. Mousavi, J. Ashdown, and K. Turk, "An autonomous spectrum management scheme for unmanned aerial vehicle networks in disaster relief operations," *IEEE Access*, vol. 8, pp. 58 064–58 079, 2020.
- [12] A. Viseras, J. Marchal, M. Schaab, J. Pages, and L. Estivill, "Wildfire monitoring and hotspots detection with aerial robots: Measurement campaign and first results," in 2019 IEEE International Symposium on Safety, Security, and Rescue Robotics (SSRR). IEEE, 2019, pp. 102– 103.
- [13] E. T. Alotaibi, S. S. Alqefari, and A. Koubaa, "LSAR: Multi-UAV collaboration for search and rescue missions," *IEEE Access*, vol. 7, pp. 55 817–55 832, 2019.
- [14] S. Enayati, H. Saeedi, H. Pishro-Nik, and H. Yanikomeroglu, "Moving aerial base station networks: A stochastic geometry analysis and design perspective," *IEEE Transactions on Wireless Communications*, vol. 18, no. 6, pp. 2977–2988, June 2019.
- [15] Y. Zeng, J. Xu, and R. Zhang, "Energy minimization for wireless communication with rotary-wing UAV," *IEEE Transactions on Wireless Communications*, vol. 18, no. 4, pp. 2329–2345, 2019.
- [16] S. Srigrarom, N. J. L. Sie, H. Cheng, K. H. Chew, M. Lee, and P. Ratsamee, "Multi-camera multi-drone detection, tracking and localization with trajectory-based re-identification," in 2021 Second International Symposium on Instrumentation, Control, Artificial Intelligence, and Robotics (ICA-SYMP). IEEE, 2021, pp. 1–6.
- [17] D. Wierzbicki, "Multi-camera imaging system for UAV photogrammetry," Sensors, vol. 18, no. 8, p. 2433, 2018.